

# Calibration of Hypoplastic Parameters – Two Different Aspects

Amir Mosallaei<sup>1\*</sup>, András Mahler<sup>1</sup>

<sup>1</sup> Department of Engineering Geology and Geotechnics, Faculty of Civil Engineering, Budapest University of Technology and Economics, Műegyetem rkp. 3, H-1111 Budapest, Hungary

\* Corresponding author, e-mail: [mosallaei@edu.bme.hu](mailto:mosallaei@edu.bme.hu)

Received: 27 November 2024, Accepted: 26 January 2024, Published online: XX XXXXXXX 2024

## Abstract

Numerical modeling serves as a widely utilized method for addressing geotechnical concerns. A pivotal aspect of this modeling process is the accurate characterization of material behavior. The connection between stress and strain tensors within soil is explicated by the soil constitutive equation, which is reliant on factors like soil type and deformation circumstances. One notable model is hypoplasticity, which has been in use for more than three decades. This research aims to calibrate the hypoplastic parameters for Danube sand using the SoilTest Module of PLAXIS. The constitutive hypoplastic model for Danube sand was fine-tuned through a series of numerical simulations. The parameter calibration occurred twice: initially according to 5 cycles of hysteresis loop of stress–strain diagram of cyclic triaxial testing, and then subsequently in accordance with strain trends observed after ten thousand cycles. A comparison was drawn between parameters determined from the overall strain trends and those calibrated based on the five cycles. The findings indicate that while the model calibrated during a specific segment of testing can accurately predict strain values during compression and extension, it falls short in forecasting the accumulated settlement following prolonged cyclic loading. This suggests the model's limited capability in anticipating long-term cyclic load effects on settlement behavior.

## Keywords

hypoplasticity, intergranular strain, cyclic triaxial test, Danube sand, SoilTest Module

## 1 Introduction

Since the beginning of geotechnical numerical modeling, there has been a demand to use material models that adequately describe the soil's behavior in the computations. The appropriate material model is determined not only by the type of soil but also by the geotechnical task to be investigated. Different material models or model parameters may be necessary for the same soil in case of different problems.

This research project aims to examine sand's response to cyclic loading from two separate aspects. In the case of an earthquake, for example, typically, the stress–deformation behavior resulting from a smaller number of load cycles must be examined, while, e.g., in the case of sand under a road structure, the cumulative deformations that occur as a result of several thousand passes are interesting. The main question of the research is what material model and soil parameters can be used to adequately describe the behavior of the soil in these two cases.

Cambridge soil mechanics school established the Cam-clay model [1] to predict soil behavior. Since then, several models with varying degrees of sophistication and complexity have been proposed. More advanced mathematical formulas have been introduced, as has increased the number of material parameters [2].

Although the HS small [3] material model may provide hysteretic material damping, experience has revealed that it falls short of the actual behavior at extremely small stresses. Extra damping or a new constitutive model should be absolutely essential to simulate realistic soil behavior [4].

Only a few constitutive model can effectively describe the behavior of sand. Frequent use is made of the Mohr-Coulomb model [5].

Numerous soil–structure interface models, including those based on nonlinear elasticity, damage mechanics models, state-dependent plasticity models, elastoplastic models, and models based on the disturbed state concept,

have been investigated. As a consequence, the basic models are incapable of accounting for the soil's complicated history reliance. Additionally, a new calibration of the constitutive model is required for a similar soil with various initial densities [6].

A big challenge has been figuring out how to imitate sand's state-dependent behavior [7].

It is preferable to use a constitutive model able to generating the essential aspects of material behavior, but not all features, with minimal required formulas elements. In characterizing the mechanical behavior of sands, the hypoplastic model is developed as an alternative to the prevalent elastoplastic models. Unlike loose sand, which has a constant volume change, dense sand has an initial contraction and then a dilatancy. This results in a constitutive model with an elegant mathematical formulation and only four material parameters [2].

Since the late 1970s, researchers have been working on hypoplasticity theory. Hypoplastic models have been found to work quite well for deformations caused by grain skeleton rearrangements. However, applying hypoplasticity to cyclic stressing or small-amplitude deformation revealed several flaws. The most noticeable flaw was an abnormal accumulation of deformation expected for minor stress cycles, known as ratcheting. The hypoplastic technique anticipated too much pore pressure buildup for undrained cyclic shearing. Until Niemunis and Herle [8] introduced intergranular strain parameters as a solution to the aforementioned issue, neither small-strain stiffness nor influences of recent history were well reproduced by hypoplasticity.

In order to be tested for a wide range of diverse scenarios, such models must be built and calibrated utilizing high-quality cyclic laboratory testing with a variety of boundary conditions [9, 10].

Several studies have been conducted in order to replicate and calibrate the hypoplastic parameters of various types of soil.

Herle and Gudehus [11] briefly introduced a hypoplastic model for the axially symmetric case, and described in detail a procedure for the determination of its parameters. They found out that all parameters of the hypoplastic model are closely related to the granulometric properties of grain assemblies [11].

Fu et al. [12] proposed a hypoplastic constitutive model to model the cementation-induced enhanced stiffness, strength and dilative behavior of cemented sand and gravel materials.

Kadlíček et al. [13] discussed an automated deterministic approach to parameters calibration of the hypoplastic model for sand. The calibration is performed on results from basic laboratory experiments such as the oedometric test, isotropic compression test, and the drained and undrained triaxial shear tests. The calibration method is structured in a hierarchical order and implemented into a free-to-use online application called ExCalibre. The method is based on the sensitivity study performed prior to the development of the calibration method. The calibration procedure respects the physical meaning of the calibrated parameters and their influence on the stiffness and asymptotic states, rather than performing a blind optimization of an objective function [13].

Moussa et al. [14] modified hypoplastic model to clarify the effect of stress level on shear strength and stiffness.

Stutz et al. [5] proposed a new approach for advanced interface models using hypoplasticity.

To predict the accumulated settlement for a long time period, it is necessary to define the behavior of the material accurately in the software. Finally, to have a set of hypoplastic parameters, series of laboratory measurements were done. In order to calibrate gained parameters, two different approaches were compared. First set of parameters were calibrated through long term tendency of strain. The second set of parameters were calibrated according to 5 cycles of hysteresis loop of stress–strain diagram.

## 2 Hypoplasticity

The general form of the hypoplastic constitutive equation is expressed as:

$$\dot{\mathbf{T}} = \mathbf{F}(\mathbf{T}, e, \mathbf{D}), \quad (1)$$

where the tensor function  $\mathbf{F}$  is dependent on stress  $\mathbf{T}$ , void ratio  $e$ , and stretching rate  $\mathbf{D}$ . According to the findings of Gudehus [15] and Bauer [16], the function  $\mathbf{F}$  can be formulated as:

$$\mathbf{F} := f_s(\text{tr}\mathbf{T}, e) (\mathbf{L}(\hat{\mathbf{T}}, \mathbf{D}) + f_d(\text{tr}\mathbf{T}, e) \mathbf{N}(\hat{\mathbf{T}}) \|\mathbf{D}\|). \quad (2)$$

In Eq. (2),  $\mathbf{L}$  and  $\mathbf{N}\|\mathbf{D}\|$  are tensorial parts dependent on  $\mathbf{D}$  and  $\hat{\mathbf{T}}$  (stretching rate and stress ratio tensor, respectively).

$\hat{\mathbf{T}} = \mathbf{T}/\text{tr}\mathbf{T}$  is dimensionless and coaxial with  $\mathbf{T}$ . The scalar quantities  $f_s$  and  $f_d$  represent the pressure-dependent stiffness factor and density factor, respectively.

In the context of this research, an axially symmetric compression condition, sufficient for determining model

parameters, is considered. The tensorial equation is divided into two scalar expressions [17].

$$\dot{T}_{s1} = f_s \frac{(T_{s1} + 2T_{s2})^2}{T_{s1}^2 + 2T_{s2}^2} \left[ \begin{aligned} &D_1 + a^2 \frac{T_{s1}D_1 + 2T_{s2}D_2}{(T_{s1} + 2T_{s2})^2} T_{s1} \\ &+ f_d \frac{a}{3} \frac{5T_{s1} - 2T_{s2}}{T_{s1} + 2T_{s2}} \sqrt{D_1^2 + 2D_2^2} \end{aligned} \right] \quad (3)$$

$$\dot{T}_{s2} = f_s \frac{(T_{s1} + 2T_{s2})^2}{T_{s1}^2 + 2T_{s2}^2} \left[ \begin{aligned} &D_2 + a^2 \frac{T_{s1}D_1 + 2T_{s2}D_2}{(T_{s1} + 2T_{s2})^2} T_{s2} \\ &+ f_d \frac{a}{3} \frac{4T_{s2} - 2T_{s1}}{T_{s1} + 2T_{s2}} \sqrt{D_1^2 + 2D_2^2} \end{aligned} \right] \quad (4)$$

In Eqs. (3) and (4), the subscript 1 represents the axial direction, while subscript 2 represents the radial direction [11]. The scalar factors  $f_s$  and  $f_d$  incorporate the impact of mean skeleton pressure  $P_s = -(T_{s1} + 2T_{s2})/3$ , and void ratio  $e$ :

$$f_s = \frac{\frac{h_s}{n} \left(\frac{e_i}{e}\right)^\beta \frac{1+e_i}{e_i} \left(\frac{3P_s}{h_s}\right)^{1-n}}{3 + a^2 - a\sqrt{3} \left(\frac{e_{i0} - e_{d0}}{e_{c0} - e_{d0}}\right)^\alpha}, \quad (5)$$

$$f_d = \left(\frac{e - e_d}{e_c - e_d}\right)^\alpha, \quad (6)$$

$$a = \frac{\sqrt{3}(3 - \sin \varphi_c)}{2\sqrt{2} \sin \varphi_c}. \quad (7)$$

The hypoplastic model for sand is comprised of eight parameters that can be divided into four major categories. The first category pertains to the critical friction angle, denoted as  $\varphi_c$ . The second category includes two parameters:  $h_s$ , which stands for granular stiffness, and  $n$ , which serves as an exponent for  $h_s$ . The third category is dedicated to various types of void ratios, where  $e_{d0}$  represents the minimum void ratio at zero pressure,  $e_{c0}$  represents the critical void ratio at zero pressure, and  $e_{i0}$  represents the maximum void ratio at zero pressure. The fourth and final category encompasses the last two parameters,  $\alpha$  and  $\beta$ , which respectively impact the peak of the friction angle and control the stiffness. Wolfersdorff's hypoplastic model is used in this paper [17].

## 2.1 Critical friction angle

The parameter  $\varphi_c$  represents the critical angle of internal friction, which is a fundamental parameter in soil mechanics and geotechnical engineering. It describes

the minimum angle at which a soil mass will fail or slide under shear stress and determines the soil's shear strength.

In coarse-grained soils, the angle of repose test is a straightforward method for determining  $\varphi_c$ . However, for soils with a larger proportion of fine grains, triaxial shear tests on normally consolidated samples are recommended.

Measuring the angle of repose can approximate the critical friction angle for soils with grain sizes larger than 0.1 mm, while the funnel method is preferred for sand soil. The funnel test involves slowly lifting a funnel filled with soil to create a heap close to critical state. Contact between the funnel and forming heap should be constant and the base beneath the heap should be rough to prevent sliding [13].

## 2.2 Granulate hardness and its exponent

The measurement of granulate hardness is valuable for gathering information on the particle size distribution, packing density, and flow characteristics of the material, which can aid in optimizing handling and processing operations.

Performing an oedometer test yields plotting the compression curve. Calculation of the exponent  $n$  is the first step, as it is not dependent on the parameter  $h_s$ . Determination of  $n$  is crucial in determining  $h_s$ .

Granular hardness  $h_s$  is the only parameter with the dimension of stress and should not be confused with the hardness of individual grains. The exponent  $n$  takes into account the pressure-sensitivity of the grain skeleton, allowing for a non-proportional increase in incremental stiffness with increasing pressure. An oedometer test is simpler than isotropic compression for determining  $h_s$  and  $n$ , with a dry or water-saturated specimen used to suppress physico-chemical effects. Parameters  $h_s$  and  $n$  control the slope and curvature of the compression line, respectively [11, 13].

## 2.3 Minimum, critical and maximum void ratio at zero pressure

Generally, the most effective way to achieve optimal compaction of a granular soil is by applying cyclic shearing with small amplitude under constant pressure. When this technique is implemented following static compression, it will gradually approach a minimum void ratio  $e_d$  which decreases with increasing pressure. Equation (8) can be used to describe the relationship between  $e_d$  and  $p_s$ , enabling the extrapolation of the value of  $e_d$  at zero pressure.

$$e_{d0} = e_d \exp \left[ \left( \frac{3p_s}{h_s} \right)^n \right] \quad (8)$$

Typically, a minimum void ratio  $e_{\min}$  is determined using index tests outlined in several standards. However, these tests are not as efficient as cyclic shearing. As a result, the measured value of  $e_{\min}$  may be higher than that of  $e_d$ . Upon comparing  $e_{d0}$  with  $e_{\min}$ , it is found that they are relatively similar, with  $e_{\min}$  being slightly higher than  $e_{d0}$ . Therefore, in the absence of data for  $e_{d0}$ ,  $e_{\min}$  can be used as a substitute [11].

Similar to  $e_{d0}$ , the critical void ratio value at zero pressure can be computed. The parameter  $e_c$  can be determined through a shear test on a soil element while calculating  $\varphi_c$ . An undrained triaxial test is usually sufficient for establishing  $e_c$ . It has been noted that the value of  $e_{c0}$  is comparable to  $e_{\max}$ .

Previously, Herle and Gudehus [11] indicated a narrow range of 0.52 to 0.64 for the ratio of  $e_{d0}/e_{c0}$ . Mašin [18] also proposed an empirical formula of  $e_{d0} = 0.5 * e_{c0}$  to be used when experimental data is not available.

The parameter  $e_{i0}$  represents the highest possible void ratio of a basic grain skeleton achieved during an isotropic consolidation of a grain suspension in an environment without gravity.

The maximal void ratio  $e_{\max}$  can be determined through various laboratory methods and is typically denser than the theoretical maximum. Empirically,  $e_{d0}/e_{\max}$  ratios of 1.2 for spheres and 1.3 for cubes have been found [11, 13].

## 2.4 Exponent $\alpha$ and $\beta$

The stiffness and pyknotropy factors are controlled by parameters  $\alpha$  and  $\beta$ , which can be determined through a parametric study involving simulations of the triaxial shear test. To obtain  $\alpha$ , Herle and Gudehus [11] suggests using Eq. (9) and considering the peak state in a triaxial compression test.

$$\alpha = \frac{\ln \left[ 6 \times \frac{(2 + K_p)^2 + a^2 K_p (K_p - 1 - \tan v_p)}{a(2 + K_p)(5K_p - 2) \sqrt{4 + 2(1 + \tan v_p)^2}} \right]}{\ln \frac{e - e_d}{e_c - e_d}} \quad (9)$$

Equation (9) involves  $K_p$ ,  $a$  and  $v_p$ , which can be calculated using Eqs. (10), (11), and (13), respectively.

$$K_p = \frac{1 + \sin \varphi_p}{1 - \sin \varphi_p} \quad (10)$$

$$a = \frac{\sqrt{3}(3 - \sin \varphi_c)}{2\sqrt{2} \sin \varphi_c} \quad (11)$$

$$A = \frac{a^2}{(2 + K_p)^2} \left[ 1 - \frac{K_p(4 - K_p)}{5K_p - 2} \right] \quad (12)$$

$$\tan v_p = 2 \frac{K_p - 4 + 5AK_p^2 - 2AK_p}{(5K_p - 2)(1 + 2A)} - 1 \quad (13)$$

To determine  $v_p$ , Eq. (13) can be used to calculate parameter  $A$ . The evaluation of  $\alpha$  and  $\beta$  requires knowledge of these preceding parameters.

The parameter  $\beta$  is significant only when the void ratio  $e$  is significantly lower than the initial void ratio  $e_i$ . According to Herle and Gudehus [11], for natural sands, assuming  $\beta = 1$  is usually adequate, regardless of granulometric properties.

A drained triaxial test on a dense sample and curve simulation using various amounts of  $\alpha$  can be conducted to calibrate these parameters. Fitting the resulting curves will yield the optimal value for  $\alpha$ . increasing  $\alpha$  decreases the stress peak on the stress–strain curve, while  $\beta$  changes the location of the peak by reducing the strain value and shifting the peak to the left.

## 3 Intergranular strain

The basic hypoplastic models are inadequate in predicting high initial stiffness and ratcheting, which is the accumulation of strains in stress cycles and stresses in strain cycles. The intergranular strain concept is the most widely used approach to overcome this limitation. The concept assumes that reversible deformation of the intergranular strain layer, combined with elastic deformation of the grains, accounts for all measured soil deformation at the beginning of the loading process until a certain amount of strain is reached and grains start to rearrange. This reversible deformation is described by an additional component of the model, while the deformation associated with grain rearrangement is irreversible and predicted by the standard hypoplastic model.

The intergranular formulation is presented in this context to incorporate extra parameters as detailed by Niemunis and Herle [8].

$$\mathbf{M} = \left[ \rho^\chi m_T + (1 - \rho^\chi) m_R \right] \mathbf{L} + \begin{cases} \rho^\chi (1 - m_T) \mathbf{L} : (\hat{\delta} \hat{\delta}) + \rho^\chi N \hat{\delta} & \text{for } \hat{\delta} : \mathbf{D} > 0 \\ \rho^\chi (m_R - m_T) \mathbf{L} : (\hat{\delta} \hat{\delta}) & \text{for } \hat{\delta} : \mathbf{D} \leq 0 \end{cases} \quad (14)$$

$\mathbf{M}$  represents a fourth-order tensor indicating the stiffness derived from the hypoplastic tensor. Introducing the intergranular strain adds five more parameters to the basic

parameters, namely  $m_R$ ,  $m_T$ ,  $\beta_r$ ,  $R$ , and  $\chi$ , which are discussed in detail in the following sections.

To address the issue of ratcheting, Niemunis and Herle [8] introduced an intergranular strain into a hypoplastic constitutive model, wherein this supplementary state variable captures the deformation occurring within the interface layer between grains. Poblete et al. [19] subjected a sample of soil to multidimensional cyclic loading when two or three principal components of the stress or strain tensor were simultaneously controlled to perform a repetitive path. Fuentes et al. extended hypoplastic model for sands combined with the intergranular strain anisotropy to account for cyclic mobility effects to allow for the simulation of liquefaction phenomena [20].

Mašin explained the structure of the mathematical formulation of hypoplasticity [18], while Namaei-kohal et al. [21] calibrated Tehran silica sand for a hypoplastic soil constitutive model with intergranular strain.

Mohammadi-Haji and Ardakani [22] conducted a series of laboratory experiments on Firoozkuh sand, followed by numerical simulations, to ascertain the parameters of a comprehensive hypoplastic constitutive model for sand. Niemunis et al. [23] presented a high-cycle explicit model for the accumulation of strain in sand due to small cyclic loading.

Yang et al. [24] proposed a hypoplastic constitutive model for granular soils grounded in the newly developed anisotropic critical state theory. This model concurrently satisfies the conditions of fabric anisotropy along with traditional conditions at the critical state [24]. Sturm [25] presented a stability criterion for shallow foundations on sand for various loading conditions. Arnold [26] extended hypoplastic constitutive models by incorporating an elastic strain range into an existing hypoplastic interface model.

### 3.1 Stiffness factor

The parameter called  $m_R$  is responsible for controlling the strength of the shear modulus at very small strain values, both during initial loading and when the strain path direction is reversed by 180 degrees. The most accurate way to determine the value of  $m_R$  is through shear wave propagation experiments, such as bender element tests. However, it is also possible to measure the shear modulus using static shear tests, although this method is less reliable as it relies on local measurements of sample deformation and strain transducers have a limit of accuracy [18].

### 3.2 Parameter $m_T$

Determining the value of parameter  $m_T$  (or ratio  $m_{rat} = m_T/m_R$ ) through experimentation is challenging.

The  $m_{rat}$  value is equivalent to the ratio of initial shear stiffness after a 90-degree change in strain path direction  $G_{90}$  to the initial stiffness  $G_0$ , expressed as  $G_{90}/G_0$ .  $G_{90}$  cannot be measured through wave propagation techniques and requires accurate measurements using local strain transducers. However, if such experiments are not feasible for a particular soil, a standard value of  $m_{rat}$  is recommended. A default value of 0.7 is commonly used for  $m_{rat}$  if there is no experimental data available for the soil of interest [18].

### 3.3 Elastic strain amplitude, intergranular strain hardening parameter and exponent

The intergranular strain concept model utilizes three parameters, namely  $R$ ,  $\beta_r$ , and  $\chi$ , each with a distinct physical interpretation. The parameter  $R$  specifies the extent of the elastic range in the strain space, whereas  $\beta_r$  controls the rate of evolution of the intergranular strain tensor. On the other hand,  $\chi$  regulates the interpolation between the reversible elastic and nonlinear hypoplastic response. Despite their varied interpretations, these parameters work together to determine the rate of stiffness degradation with increasing strain, which, in turn, affects the predictions of the model. The calibration of these parameters usually involves triaxial shear experiments that measure local deformation and obtain shear modulus versus shear strain curves. An increase in  $R$  causes a decrease in  $\beta_r$  and shifts the stiffness degradation curve horizontally in the  $G$  versus  $\ln(\varepsilon_s)$  diagram. Conversely,  $\chi$  influences the rate of stiffness decrease with strain and a higher  $\chi$  value leads to a larger quasi-elastic range size and a faster subsequent rate of stiffness decrease. To calibrate the  $\chi$  parameter, an experimental trial-and-error process is required to fit the data.

According to Mašin [18], it is difficult to differentiate the influence of  $m_R$ ,  $\beta_r$ , and  $\chi$  on the accumulation of strain caused by cyclic loading. Hence, he suggested a calibration method that involves treating  $R = 10^{-4}$  and  $\chi = 1$  as constants independent of the material. Then,  $m_R$  can be calibrated using bender element measurements, which are relatively simple to perform. Moreover,  $m_T$  can be set to  $0.7 * m_R$ . Finally, the cyclic behavior can be controlled by adjusting only the parameter  $\beta_r$ .

## 4 Results and discussion

### 4.1 Sieve test

In order to have the particle size distribution, laboratory measurement was done according to ISO 17892-4:2016 [27]. Fig. 1 is presenting the particle size distribution of the Danube granular material which was used as the sample. Table 1 announced the portion of the sand and silt in the sample.

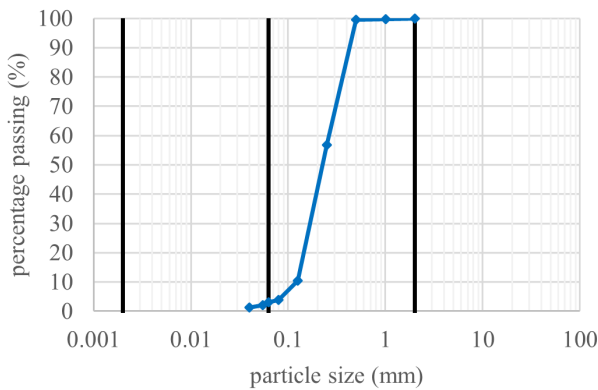


Fig. 1 Soil particle size distribution curve

Table 1 Percentage of soil particles

Gr	Sa	Si	Cl
0%	97.38%	2.62%	0%

#### 4.2 Oedometer test

To have the stress and relative void ratio, oedometer test was conducted using ISO 17892-5:2017 [28]. Table 2 demonstrate the result of the oedometer test.

#### 4.3 Minimum and maximum void ratio $e_{min}$ , $e_{max}$

Maximum and minimum void ratio were found during respectively minimum and maximum density. This investigation was done by the instruction which was published in DIN 18126:1996-11 [29]. So  $e_{min}$  is equal to 0.62 and  $e_{max}$  is distinguished as 1.01.

#### 4.4 Triaxial test

Consolidated triaxial compression tests on water saturated samples were done by using ISO 17892-9:2018 [30] as the instruction method. Fig. 2 illustrates the stress–strain

Table 2 Result of oedometer test

Vertical stress (kPa)	2	100	200	400	800
Void ratio	0.73	0.71	0.7	0.69	0.67

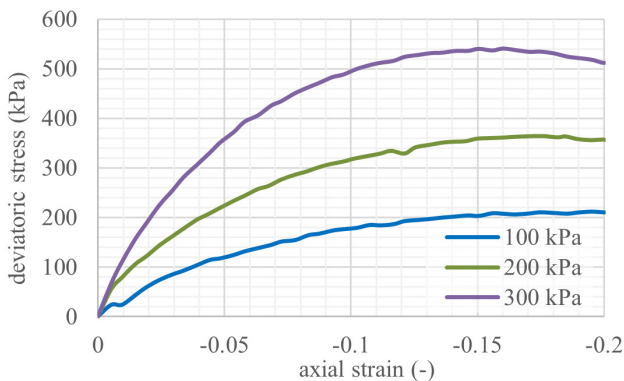


Fig. 2 Monotonic triaxial test performed in different confining pressure

curve for the three tests which were conducted with 100, 200 and 300 kPa as confining pressure.

#### 4.5 Cyclic triaxial test

Cyclic loading caused by earthquakes, wind, waves, and traffic can increase pore water pressure and accumulate plastic deformation in soil, resulting in softening of the stiffness and a reduction of soil strength; these catastrophes would result in numbers of issues such as safety reduction and environmental issues. As a result, it is critical to investigate the mechanical response of soils under cyclic loading [31].

As previously mentioned, even in the case of the same soil, different parameters may be necessary for different design purposes. In the case of cyclic loading, the stress–strain relationship that develops during the load cycles, or the accumulated deformations caused by the large number of repetitions, may arise as a question. First, the parameters were calibrated so that the material model could reasonably estimate the cumulative deformations. The complete matching of the measured and simulated results could not be achieved due to the different shapes of the curves. Therefore, the calibration was performed so that the calculation results match the trends developing after approximately 1000 cycles. The determined parameters are shown in Tables 3 and 4; with the help of such a combination of parameters, cumulative deformations occurring in a layer below the pavement could be estimated (e.g., in a layer of a road structure where a large number of load cycles are expected). The measured and calculated results are shown in Fig. 3; it can be seen that after the initial deviation, the same trends emerge, and the two curves run parallel to each other.

After that, we examined how well these parameters can reproduce the stress–deformation relationship that can be experienced during one cycle Fig. 4.

It can be seen that the parameter set fails to predict the stress–strain relationship in one cycle. After that, we performed the calibration of the intergranular strain parameters

Table 3 Hypoplastic parameters of Danube sand calibrated according to the strain in 10000 cycles

$\varphi_c$	$h_s$	$n$	$e_{d0}$	$e_{c0}$	$e_{i0}$	$\alpha$	$\beta$
27.89	3.08	0.30	0.62	0.971	1.2	0.3	1.1

Table 4 Intergranular strain parameters of Danube sand calibrated according to the strain in 10000 cycles

$m_R$	$m_T$	$R_{max}$	$\beta_r$	$\chi$
5.6	3.5	2.2e-4	0.2	1.3

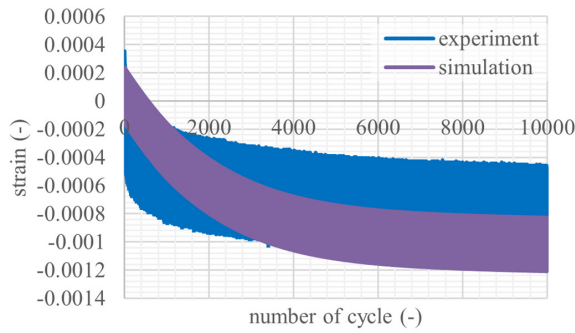


Fig. 3 Simulated and measured value of strain over time

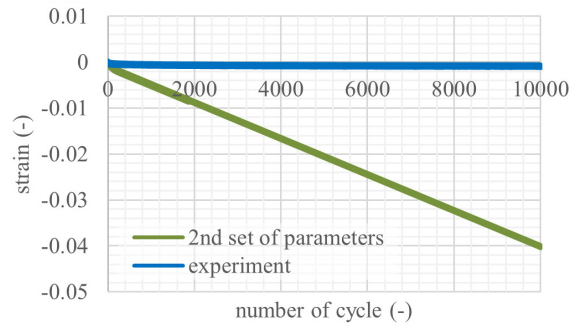


Fig. 6 Simulated strain over time according to approach B

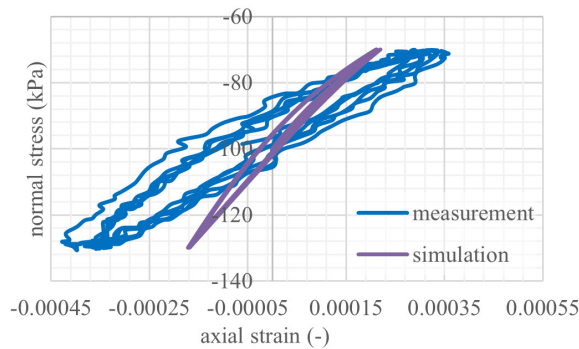


Fig. 4 Hysteresis loop of the first 5 cycles according to approach A during cyclic triaxial test

in such a way that they would describe the stress–strain relationship of the examined cycle. The parameters determined in this way can be seen in Table 5, and the curves of the stress–strain of the first five cycles are shown in Fig. 5.

Fig. 6 shows how the cumulative deformations develop with these parameters. In this case, the calculation significantly overestimates the deformations that develop in the long term.

Table 5 Intergranular strain parameters of Danube sand calibrated according to the hysteresis loop of first 5 regular cycles

$m_R$	$m_T$	$R_{max}$	$\beta_r$	$\chi$
3.4	2	1.9e-4	0.3	1.3

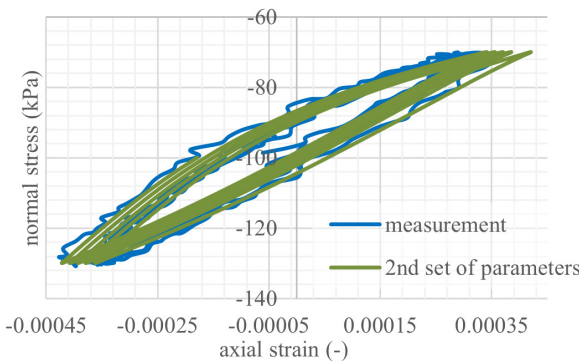


Fig. 5 Hysteresis loop of the first 5 cycles according to approach B during cyclic triaxial test

Based on the performed parameter calibrations, it can be stated that the description of the short-term and long-term behavior cannot be solved with the help of a single parameter set. It is necessary to use different parameters if we perform tests for the former or the latter purpose.

### 5 Conclusions

In conclusion, this paper presents a comprehensive calibration of the hypoplastic constitutive model incorporating intergranular strain for Danube sand. The calibration process involved a combination of experimental static and dynamic soil tests, analytical solutions, and numerical simulations using SoilTest Module of PLAXIS.

The determination of hypoplastic parameters, such as  $\varphi_c$ ,  $n$ ,  $h_s$ ,  $e_{i0}$ ,  $e_{d0}$ ,  $e_{c0}$ ,  $\alpha$ , and  $\beta$ , was achieved through drained triaxial and oedometer testing. Adjustments to  $\alpha$  and  $\beta$  were made to ensure a robust fit between simulated and observed curves in drained cyclic triaxial tests.

Intergranular parameters, namely  $m_R$ ,  $m_T$ ,  $\beta_r$ ,  $R_{max}$ , and  $\chi$ , were fine-tuned using drained cyclic triaxial tests and numerical simulations to achieve an optimal fit with the strain–time curve for 10,000 cycles (calibration approach A). In the second time calibration, the adjustment was made by selecting the first five regular hysteresis loops from the stress–strain diagram of laboratory test and fitting the curve of simulated test and the intergranular parameters were adjusted based on these chosen loops (calibration approach B).

It is concluded that the hypoplastic material model is suitable for both describing the short-term behavior (i.e., a few cycles) and estimating the cumulative deformation resulting from a large number of load cycles. It has also been stated that one parameter set can be reliably used for one purpose only. Although the parameters determined by method A approximate the cumulative deformations well, they fail to describe the first few cycles appropriately. The parameters determined by procedure B are suitable

for describing the soil behavior in the first cycles but significantly overestimate cumulative strain resulting from a vast number of cycles.

## References

- [1] Roscoe, K. H., Schofield, A. N., Wroth, C. P. "On the yielding of soils", *Géotechnique*, 8(1), pp. 22–53, 1958.  
<https://doi.org/10.1680/geot.1958.8.1.22>
- [2] Wu, W., Bauer, E. "A simple hypoplastic constitutive model for sand", *International Journal for Numerical and Analytical Methods*, 18(12), pp. 833–862.  
<https://doi.org/10.1002/nag.1610181203>
- [3] Schanz, T., Vermeer, P. A., Bonnier, P. G. "The hardening soil model: Formulation and verification, Beyond 2000 Comput", In: *Beyond 2000 in Computational Geotechnics Ten Years PLAXIS International*, Amsterdam, 1999, pp. 281–296. ISBN 90 5809 040 X  
<https://doi.org/10.1201/9781315138206-27>
- [4] Hübner, B., Mahler, A. "Analysis of Seismic Fragility Functions of Highway Embankments", *Periodica Polytechnica Civil Engineering*, 64(4), pp. 1162–1169, 2020.  
<https://doi.org/10.3311/PPci.16483>
- [5] Stutz, H., Mašin, D., Sattari, A. S., Wuttke, F. "A general approach to model interfaces using existing soil constitutive models application to hypoplasticity", *Computers and Geotechnics*, 87, pp. 115–127, 2017.  
<https://doi.org/10.1016/j.compgeo.2017.02.010>
- [6] Wu, W., Lin, J., Wang, X. "A basic hypoplastic constitutive model for sand", *Acta Geotechnica*, 12(6), pp. 1373–1382, 2017.  
<https://doi.org/10.1007/s11440-017-0550-4>
- [7] Wei, X., Chen, Y., Yang, J. "A unified critical state constitutive model for cyclic behavior of silty sands", *Computers and Geotechnics*, 127, 103760, 2020.  
<https://doi.org/10.1016/j.compgeo.2020.103760>
- [8] Niemunis, A., Herle, I. "Hypoplastic model for cohesionless soils with elastic strain range", *Mechanics of Cohesive-frictional Materials*, 2(4), pp. 279–299, 1998.  
[https://doi.org/10.1002/\(SICI\)1099-1484\(199710\)2:4<279::AID-CFM29>3.0.CO;2-8](https://doi.org/10.1002/(SICI)1099-1484(199710)2:4<279::AID-CFM29>3.0.CO;2-8)
- [9] Wichtmann, T., Triantafyllidis, T. "Monotonic and cyclic tests on kaolin: a database for the development, calibration and verification of constitutive models for cohesive soils with focus to cyclic loading", *Acta Geotechnica*, 13(5), pp. 1103–1128, 2018.  
<https://doi.org/10.1007/s11440-017-0588-3>
- [10] Gajári, G., Kisgyörgy, L., Ádány, S., Mahler, A., Lógó, J., "A visco-hypoplastic constitutive model for rolled asphalt", *Periodica Polytechnica Civil Engineering*, 65(3), pp. 798–809, 2021.  
<https://doi.org/10.3311/PPci.17515>
- [11] Herle, I., Gudehus, G. "Determination of parameters of a hypoplastic constitutive model from properties of grain assemblies", *Mechanics of Cohesive-frictional Materials*, 4(5), pp. 461–486, 1999.  
[https://doi.org/10.1002/\(SICI\)1099-1484\(199909\)4:5<461::AID-CFM71>3.0.CO;2-P](https://doi.org/10.1002/(SICI)1099-1484(199909)4:5<461::AID-CFM71>3.0.CO;2-P)
- [12] Fu, Z., Chen, S., Zhong, Q., Ji, E. "A damage hypoplasticity constitutive model for cemented sand and gravel materials", *Acta Geotechnica*, 17(1), pp. 1–18, 2021.  
<https://doi.org/10.1007/s11440-021-01206-9>
- [13] Kadlíček, T., Janda, T., Šejnoha, M. "Calibration of Hypoplastic Models for Soils", *Applied Mechanics and Materials*, 821, pp. 503–511.  
<https://doi.org/10.4028/www.scientific.net/amm.821.503>
- [14] Moussa, A., Salah, M., Rafik, D. "Improvement of a Hypoplastic Model for Granular Materials Under High-Confining Pressures", *Geotechnical and Geological Engineering*, 38(4), pp. 3761–3771, 2020.  
<https://doi.org/10.1007/s10706-020-01256-y>
- [15] Gudehus, G. "Comprehensive Constitutive Equation for Granular Materials", *Soils and Foundations*, 36(1), pp. 1–12, 1996.  
<https://doi.org/10.3208/sandf.36.1>
- [16] Bauer, E. "Calibration of a Comprehensive Hypoplastic Model for Granular Materials", *Soils and Foundations*, 36(1), pp. 13–26, 1996.  
<https://doi.org/10.3208/sandf.36.13>
- [17] von Wolfersdorff, P. A. "Hypoplastic relation for granular materials with a predefined limit state surface", *Mechanics of Cohesive-frictional Materials*, 1(3), pp. 251–271, 1996.  
[https://doi.org/10.1002/\(SICI\)1099-1484\(199607\)1:3<251::AID-CFM13>3.0.CO;2-3](https://doi.org/10.1002/(SICI)1099-1484(199607)1:3<251::AID-CFM13>3.0.CO;2-3)
- [18] Mašin, D. "Modelling of Soil Behaviour with Hypoplasticity: Another Approach to Soil Constitutive Modelling", Springer Cham, 2019. ISBN 978-3-030-03976-9  
<https://doi.org/10.1007/978-3-030-03976-9>
- [19] Poblete, M., Fuentes, W., Triantafyllidis, T. "On the simulation of multidimensional cyclic loading with intergranular strain", *Acta Geotechnica*, 11(6), pp. 1263–1285, 2016.  
<https://doi.org/10.1007/s11440-016-0492-2>
- [20] Fuentes, W., Wichtmann, T., Gil, M., Lascarro, C. "ISA-Hypoplasticity accounting for cyclic mobility effects for liquefaction analysis", *Acta Geotechnica*, 15(6), pp. 1513–1531, 2020.  
<https://doi.org/10.1007/s11440-019-00846-2>
- [21] Namaei-kohal, A., Ardakani, A., Hassanlourad, M. "Hypoplastic soil model parameters calibration for Tehran silica sand and verification with a monotonic geocell pullout test", *Arabian Journal of Geosciences*, 15(9), 824, 2022.  
<https://doi.org/10.1007/s12517-022-10110-9>
- [22] Mohammadi-Haji, B., Ardakani, A. "Calibration of a Hypoplastic Constitutive Model with Elastic Strain Range for Firoozkuh Sand", *Geotechnical and Geological Engineering*, 38(5), pp. 5279–5293, 2020.  
<https://doi.org/10.1007/s10706-020-01363-w>
- [23] Niemunis, A., Wichtmann, T., Triantafyllidis, T. "A high-cycle accumulation model for sand", *Computers and Geotechnics*, 32(4), pp. 245–263, 2005.  
<https://doi.org/10.1016/j.compgeo.2005.03.002>
- [24] Yang, Z., Liao, D., Xu, T. "A hypoplastic model for granular soils incorporating anisotropic critical state theory", *International Journal for Numerical and Analytical Methods in Geomechanics*, 44(6), pp. 723–748, 2020.  
<https://doi.org/10.1002/nag.3025>

In the case of a specific task, it is therefore necessary to calibrate the parameters and perform the calculations, considering the engineering questions to be answered.

- [25] Sturm, H. "Numerical investigation of the stabilisation behaviour of shallow foundations under alternate loading", *Acta Geotechnica*, 4(4), pp. 283–292, 2009.  
<https://doi.org/10.1007/s11440-009-0102-7>
- [26] Arnold, M. "Application of the intergranular strain concept to the hypoplastic modelling of non-adhesive interfaces", In: *The 12th International Conference of International Association for Computer Methods and Advances in Geomechanics*, Goa, India, 2008, pp. 747–754. ISBN 9781622761760
- [27] ISO "ISO 17892-4:2016 - Geotechnical investigation and testing — Laboratory testing of soil — Part 4: Determination of particle size distribution", International Organization for Standardization, Geneva, Switzerland, 2016. [online] Available at: <https://www.iso.org/standard/55246.html>
- [28] ISO "ISO 17892-5:2017 - Geotechnical investigation and testing — Laboratory testing of soil — Part 5: Incremental loading oedometer test", International Organization for Standardization, Geneva, Switzerland, 2017. [online] Available at: <https://www.iso.org/standard/55247.html>
- [29] DIN "DIN 18126:1996-11 Baugrund, Untersuchung von Bodenproben - Bestimmung der Dichte nichtbindiger Böden bei lockerster und dichtester Lagerung" (Soil, investigation and testing - Determination of density of non-cohesive soils for maximum and minimum compactness), Deutsches Institut für Normung, Berlin, Germany, 1996. (in German)  
<https://doi.org/10.31030/7209583>
- [30] ISO "ISO 17892-9:2018 - Geotechnical investigation and testing — Laboratory testing of soil — Part 9: Consolidated triaxial compression tests on water saturated soils", International Organization for Standardization, Geneva, Switzerland, 2018. [online] Available at: <https://www.iso.org/standard/70954.html>
- [31] Yin, Z.-Y., Hicher, P.-Y., Jin, Y.-F. "Practice of Constitutive Modelling for Saturated Soils", In: *Practice of Constitutive Modelling for Saturated Soils*, Springer Singapore, 2020. pp. 1–46. ISBN 978-981-15-6307-2  
[https://doi.org/10.1007/978-981-15-6307-2\\_1](https://doi.org/10.1007/978-981-15-6307-2_1)